Journal Pre-proofs

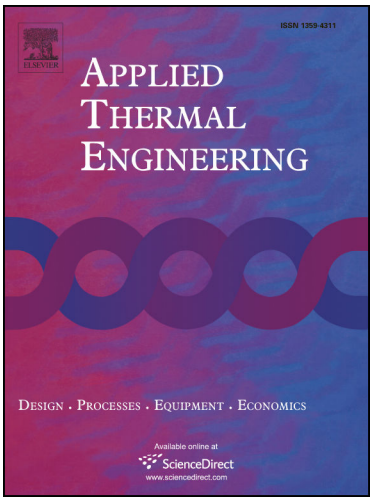

Development of structural layers PVC incorporating phase change materials for thermal energy storage

C. Amaral, N.V. Gama, F. Mohseni, J.S. Amaral, V.S. Amaral, P.A.A.P. Marques, A. Barros-Timmons, R. Vicente

PII: S1359-4311(20)33189-6
DOI: https://doi.org/10.1016/j.applthermaleng.2020.115707
Reference: ATE 115707

To appear in: *Applied Thermal Engineering*

Received Date: 1 October 2019
Revised Date: 1 July 2020
Accepted Date: 3 July 2020

Please cite this article as: C. Amaral, N.V. Gama, F. Mohseni, J.S. Amaral, V.S. Amaral, P.A.A.P. Marques, A. Barros-Timmons, R. Vicente, Development of structural layers PVC incorporating phase change materials for thermal energy storage, *Applied Thermal Engineering* (2020), doi: https://doi.org/10.1016/j.applthermaleng.2020.115707

Development of structural layers PVC incorporating phase change materials for thermal energy storage

C. Amaral[1], N. V. Gama[2], F. Mohseni[3], J. S. Amaral[3], V. S. Amaral[3], P.A.A.P. Marques[4], A. Barros-Timmons[2], R. Vicente[1]

[1]*RISCO, Civil Engineering Department, University of Aveiro (UA), 3810-193 Aveiro, Portugal*

[2]*CICECO - Aveiro Institute of Materials and Department of Chemistry, University of Aveiro (UA), 3810-193 Aveiro, Portugal.*

[3]*CICECO - Aveiro Institute of Materials and Department of Physics, University of Aveiro (UA), 3810-193 Aveiro, Portugal*

[4]*TEMA, Department of Mechanical Engineering, University of Aveiro (UA), 3810-193 Aveiro, Portugal*

[*] *Tel.: +351 234 370 845, Fax: +351 234 370 094, e-mail: claudiaamaral@ua.pt*

Abstract

The use of poly(vinyl chloride) (PVC) structural layers incorporating phase change materials (PCM) for latent heat thermal energy storage (LHTES) has become more attractive in the recent years compared to other supporting materials. In this study, PVC layers with different types of PCM were prepared using blending and compression moulding methods. Two types of synthesized PCM, one based on paraffin and calcium carbonate (PCM@$CaCO_3$) and the other on paraffin, silica and graphene oxide (PCM@SiGO) have been developed to enhance the thermal conductivity of the PVC matrix and thus achieve a more effective charging and discharging process. PVC layers prepared using a commercial PCM (PCM@BASF) were also prepared for comparison.

SEM images and DSC results reveal homogeneous distribution of the PCM in PVC layers and that most PCM particles are undamaged. The shell material (in the case of PCM@BASF) and the shape stability (in the case of synthesized PCM@$CaCO_3$ and PCM@SiGO) prevent leakage of molten paraffin during the PVC layer production.

The thermal conductivity profile of the PVC layer without PCM have a decreasing tendency with the temperature increase when determined using different measurement approaches, the transient plane heat source method (HotDisk Analyser, TPS 2500 S) and thermal flux meter method (steady-state method). However, for PVC layers with PCM the thermal conductivity profile shows a different behaviour when the mean surface temperature of the specimen is below the phase change transition temperature range (increasing tendency). During phase change transition (18 °C to 26 °C), the thermal conductivity presents two distinct tendencies. Firstly, the thermal conductivity reveals a decreasing tendency as the mean temperature of the specimen rises and afterwards an increasing tendency. Secondly, when the mean surface temperature is above the phase change transition temperature range, the thermal conductivity profile shows a decreasing tendency, independent of the PCM.

The mechanical properties of PVC layers were also assessed and the results obtained revealed that the incorporation of PCM into the PVC matrix reduces the mechanical performance of the

composites, however for LHETS applications not subjected to high tensile stress levels (over 1 kPa), this is not a significant drawback.

Keywords: phase change material (PCM); poly(vinyl chloride) (PVC); thermal conductivity; thermal energy storage; shape stabilized PCM.

1 Introduction

The building and industrial sectors generate pollution and consume natural resources being one of the major energy consumers taking up to 40 % of the overall energy consumption [1–4]. Therefore, thermal energy storage (TES) systems are a useful tool to improve the energy efficiency and reduce energy consumption, without compromising thermal comfort and indoor air quality in buildings [5,6]. The most attractive TES system is the latent heat storage because of high storage density and small temperature change from storage to release. In latent heat thermal energy storage (LHTES) systems, the energy of a phage change material (PCM) is stored during melting and released during cooling. Therefore, the use of PCM can increase the energy storage of building components [7–10] by storing thermal energy. Moreover, it has a thermal regulation effect by charging and discharging large amounts of latent heat during the phase change process [11–15].

PCM are divided into two main categories: organic and inorganic. This classification depends on different chemical properties. These types of materials have been studied during the last 40 years, including mainly hydrated salts, paraffin waxes, fatty acids and eutectic mixtures of organic and non-organic compounds. Paraffin has been widely used for LHTS systems [11–13,16] however, the low thermal conductivity of this type of PCM limits the full potential of this material since it slows down the heat transfer process associated with the charging and discharging processes. Hence, a variety of strategies to improve the thermal properties of PCM [5] have been tested, including: the incorporation of high thermal conductivity nanofillers or other additives [17–20], the micro/nano encapsulation of PCM with a high thermal conductive shell material [14,21–24] and the shape stabilization of the PCM with high thermal conductive supporting materials [25–27]. Vivekananthan and Amirtham [28] studied the thermal conductivity enhancement of a PCM composite dispersing three different mass fraction (0.1 wt.%, 0.5 wt.% and 1.0 wt.%) of graphene particles in the PCM matrix. It was concluded that the thermal conductivity of the PCM was enhanced with the increase of weight fraction of graphene due to its inherent high thermal conductivity (the addition of 1 wt.% of graphene led to 53.1 % increase in thermal conductivity

with only 6.1 % decrease in latent heat enthalpy). Mehrali et al. [27] studied a new shape stable composite PCM prepared by vacuum impregnation of graphene oxide (GO) sheets with paraffin. The resulting PCM composite containing 48.3 wt.% of paraffin proved to be shape stable, as leakage of PCM was not observed, whilst the thermal conductivity enhancement was 230%. The decrease in latent heat capacity values was 50% (which is acceptable for LHTES applications for composite PCM in this study). Jiang et al. [29] prepared microencapsulated PCM with calcium carbonate ($CaCO_3$) shells modified with GO using a modified self-assembly method. This microencapsulated PCM had higher thermal conductivity and better mechanical properties than the microencapsulated PCM with $CaCO_3$ shells prepared without GO. Qu et al. [30] tested two PCM composites by adding two hybrid carbon nano-additives fillers: expanded graphite-multi-walled carbon nanotube (EG-MWCNT) and expanded graphite-carbon nanofiber (EG-CNF). Whilst the mass ratios of EG-MWCNT and EG-CNF had the same effect on the thermal conductivity enhancement, the EG-MWCNT based PCM composites showed higher thermal conductivity than EG-CNF based PCM composites due to the higher thermal conductivity of MWCNT.

A shape stabilized PCM is composed of a working substance and a supporting material (prevents the melted phase from leaking). There is a variety of supporting materials that can be used for shape stabilization of PCM which includes polymer matrices, porous materials and nanomaterials [31,32]. In the case of polymeric materials, the poly(vinyl chloride) (PVC) has been explored by some researchers, as shell material in microencapsulated PCM (more efficient to prevent leakage during the melted phase than others polymeric shells) or as a supporting material in shape stabilized PCM (the PCM melts and solidifies more easily in a PVC network, keeping its shape) [33–36]. Feldman et al. [37] studied the possibility of developing shape stabilized PCM based on PVC and fatty acids. Jin et al. [38] prepared microencapsulated PCM as latent heat storage of medium of a high-density polyethylene/wood flour compound as a supporting material for potential LHTES application. Chen et al. [39] studied the development of PVC macro capsules that encapsulated paraffin directly by coating multiple layers of polyamide, silica or polydopamine. The prepared composite not only solved the problems of paraffin leakage and

hysteresis of phase transition, but also had a high phase change enthalpy. Wang et al. [40] explored a simple and environment-friendly method for the preparation of micro/nano PCM encapsulated with PVC shell with excellent energy storage performance.

Despite the examples above mentioned regarding the use of PVC in combination with PCM, the addition of microencapsulated and shape stabilized PCM to PVC layers to be used in LHTES applications has not been reported so far. This work presents and discusses the thermal performance of an alternative to conventional material matrices, specifically the thermal performance of PVC structural layers filled with a commercial PCM and two synthetized PCM formulations. PVC-PCM composites were prepared by blending and compression moulding. Two types of shape stable PCM based on paraffin and calcium carbonate (PCM@$CaCO_3$) and another based on paraffin, silica and graphene oxide (PCM@SiGO) were developed aiming to enhance the thermal conductivity and to achieve a more effective charging and discharging process of the PVC layer. The PVC layers produced were thoroughly characterized with respect to their structure, morphology, mechanical and thermal properties, using different scanning methods (SEM and EDX), tensile mechanical analyses, differential scanning calorimetry (DSC), thermogravimetric analysis (TGA), transient plane heat source method (HotDisk Analyser, TPS 2500 S) and thermal flux meter method (steady-state method). Due to the more promising results of the synthesized PCM@$CaCO_3$ and PCM@SiGO compared to the commercial PCM@BASF, this experimental work focuses on the incorporation of these PCM in PVC layers for potential LHTES applications. The results obtained indicate that the structural PVC layer combined with PCM constitutes a potential solution to increase the thermal efficiency in buildings, either new or refurbish, as a layer of a modular multifunctional panel for building envelope solutions or solely as a waterproofing layer to be applied on flat roof systems.

2 Materials and Methods

2.1 Phase change materials (PCM)

2.1.1 PCM Micronal®DS 5001X (PCM@BASF)

Microencapsulated PCM (Micronal®DS 5001X - PCM@BASF) containing paraffin wax with a melting point of 26 °C as the core material and a shell of poly(methyl methacrylate) (PMMA) was purchased from BASF (Ludwigshafen, Germany).

2.1.2 PCM with calcium carbonate (PCM@$CaCO_3$)

PCM@$CaCO_3$ containing paraffin was prepared according to the procedure described by Amaral et al. [41], using paraffin RT18HC (main peak of melting point: 18 ºC and purchased from Rubitherm (Germany).

2.1.3 PCM with silica and graphene oxide (PCM@SiGO)

The PCM with silica and GO was synthesized using paraffin RT18HC (the same as referred above), using octadecylamine (OCA) and hydrochloric acid (HCl) both purchased from Sigma-Aldrich. The GO water dispersion was purchased from Graphenea (Spain), the tetraethyl orthosilicate (TEOS) was purchased from Acros Organics and the surfactant Pluronic F-127 was purchased from BASF.

In order to improve the compatibility between paraffin and GO, the alkylamination method was used. For that purpose, an ethanolic OCA solution was added to a water dispersion of GO (4mg/mL) and stirred at room temperature (RT) during 24 h, resulting in GO_OCA. Afterwards, 20 g paraffin was added to 20 mg of GO_OCA and vigorously mixed using a mechanical stirrer (CAT R100SD overhead stirrer equipped with a polytetrafluoroethylene (PTFE) half-moon blade) using 1300 rpm during 40 min. The mixture was then further homogenized using an ultrasonic water bath during 120 min at 35 ºC (to ensure the dispersion was liquid).

PCM@SiGO containing paraffin was synthesized through the interfacial polycondensation of silica precursors pH 3.0. An oil solution was prepared by stirring 15 g of paraffin with GO_OCA and 16 mL of TEOS at 500 rpm during 45 min. An O/W emulsion was formed by dropping the oil solution into 150 mL aqueous solution containing 0.75 g of F-127 surfactant with agitation at 500 rpm. Then, the emulsification was carried out in a round-bottom flask and vigorously stirred using a mechanical stirrer at 650 rpm for 45 min. Subsequently, an HCl aqueous solution (2.0

mol/L) was used as the catalyst to initiate the condensation of silica. It was added dropwise to the emulsion at a stirring rate of 250 rpm, until pH 3.0. Then, the emulsion was continuously stirred at 35 ºC, using 500 rpm during 48 h to complete the condensation. The final product was washed several times using an ethanol/water mixture (30 wt.%) and collected by vacuum filtration. Finally, the PCM@SiGO was dried in an oven at 50 ºC, during 72 h.

2.1.4 Characterization of PCM

GO and GO_OCA FTIR spectra were collected using the ATR mode, at room temperature, between 4000 and 500 cm^{-1}, using 32 scans and a resolution of 4 cm^{-1} in a Perkin Elmer FTIR System Spectrum BX Spectrometer equipped with a single horizontal Golden Gate ATR cell. The PCM spectra were collected (using KBr disks), at room temperature, between 350 and 4000 cm^{-1}, using 64 scans and a resolution of 8 cm^{-1} in a Mattson 7000 galaxy series spectrophotometer.

The morphology (shape and size) and semi quantitative atomic composition of the PCM were analysed using SEM-EDX. Each sample was coated with carbon, being the SEM analyses carried out in a Hitachi SU 70 Bruker using an accelerating voltage of 15.0 kV. In turn, the EDX spectra were collected using a Tabletop Microscope TM4000Plus from Hitachi equipped with Bruker Quantax 75.

The bulk density of a powder is the ratio of the mass of an untapped powder specimen and its volume including the contribution of the interparticle void volume. Hence, the bulk density was determined according to [42]. The values presented correspond to the average bulk density determined for 4 specimens for each type of PCM.

Dynamic scanning calorimetry (DSC) was used to determine the energy storage properties of the PCM (melting temperature and enthalpy) in a Diamond DSC PerkinElmer, using a heating rate of 5 ºC/min, between 10 ºC to 50 ºC under nitrogen atmosphere. The DSC was calibrated with indium (heating rate of 5 ºC/min, in the range of 30 to 170 ºC) prior to measurements and the specimens were accurately weighted into an aluminium capsule (pans and covers). The accuracy/precision of the equipment is ± 0.1 ºC / ± 0.01 ºC for the temperature and <±1% /

<±0.1% for the calorimetry according to the technical data sheet of the equipment [43]. The measurements were made using three specimens for each type of PCM and averaged.

The thermal stability and chemical composition of GO, GO_OCA and the PCM was evaluated in a Netzsch 449 F3 Jupiter TG, using a scanning rate of 10 ºC/min, between 30 and 600 ºC, under a nitrogen flux of 200 mL/min. The equipment has a temperature resolution of 0.0001 K and a balance resolution of a value of 0.1 μg (over the entire weighing range) according to the technical data sheet of the equipment [44].

2.2 Structural Layer (PVC) incorporating PCM

2.2.1 Structural layer (PVC)

The PCM prepared were used to produce PVC layers according to the procedure reported by Gama et al. [45,46] using 100 parts of PVC resin (VICIR S1200 with *K* value of 70 supplied by Cires (Portugal)), 60 parts of plasticizer DOTP (dioctyl terephthalate supplied by Eastman), 10 parts of ESBO (epoxidized soybean oil supplied by Galata chemicals) and 2 parts of stabilizer Ca/Zn (FI 240 CZ supplied by Markstat). Afterwards, the PVC blend was mixed with the different types of PCM (5.0 wt.%) in a high-speed mixer, being the composite films (PVC structural layer incorporating PCM) produced in a hot press (CARVER model 3851-0) at 150 ºC, at a pressure of 3 tons, during 10 min. The designation of the composite layers is summarized in Table 1.

Table 1: Designation of the PVC layers

Name	**PVC layers**
PVC	PVC layer without PCM
PVC_5PCM@BASF	PVC layer with 5.0 wt% PCM@BASF
PVC_5PCM@$CaCO_3$	PVC layer with 5.0 wt% PCM@$CaCO_3$
PVC_5PCM@SiGO	PVC layer with 5.0 wt% PCM@SiGO

Figure 1 illustrates the PVC film layers prepared with 5.0% in weight of PCM which were characterized in detail.

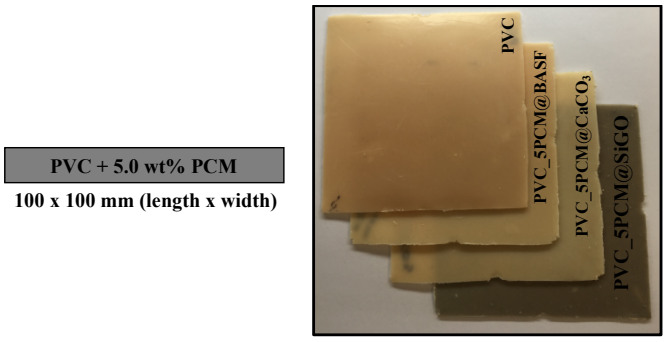

Figure 1: Image of the different PVC layers.

2.2.2 Characterization of PVC layer

The morphology (shape and size) and the composition (element types and contents) of the PVC layers were analysed by SEM and EDX. The SEM images and EDX spectra were performed using a Tabletop Microscope TM4000Plus from Hitachi equipped with Bruker Quantax 75.

The effect of the PCM on the density of the layers was determined by cutting (50×50×thickness mm^3) and weighing PVC specimens. The densities were determined dividing the weight of the specimens by their volume and the results presented correspond to the average of 3 specimens of each PVC layer. The uncertainty of the analytical scale is ± 0.0002 g while the uncertainty of digital calliper for specimen dimensions determination is ±0.01 mm. The uncertainty of the density is ±1.16 kg/m^3 and results from the propagation of uncertainty of indirect experimental measurements.

Tensile mechanical analyses of PVC layers (50x1x10 mm^3) were performed in a SHIMADZU AGS-X, using a load cell of 1.0 kN and a deformation rate of 20.0 mm/min. Three specimens of each PVC layer were tested. According to the technical data sheet of the equipment [47], the accuracy and precision of the equipment is ±1% and ±1%, respectively.

To determine the energy storage properties of the PVC layers (melting temperature and enthalpy), a dynamic scanning calorimeter (Diamond DSC, PerkinElmer) was used according to section 2.1.4. This analysis is essential to characterize the energy storage properties of the PVC layers and to determinate the PCM content ($\%_{PCM}$) incorporated in the PVC layers, according the Equation (1):

$$\%_{PCM} = \frac{\Delta H_{m,\mathrm{PCM}}}{\Delta \mathrm{H}_{m,PVC}} \times 100 \quad (1)$$

Where, $\Delta H_{m,PCM}$ corresponds to the latent heat of the PCM on heating and $\Delta H_{m,PVC}$ corresponds to the latent heat of the PVC layer with PCM.

The hot box method used to measure the thermal conductivity is based on the steady-state method. This method consists in a simple hot box configuration composed by two closed chambers with controlled temperature and relative humidity conditions: one of the chambers is at low and constant temperature (cold chamber) and the other, the measuring chamber, is placed at higher and constant temperature (warm chamber). Between the two compartments or chambers there is a mounting ring with the wall specimen or panel to be tested. The procedures, the schemes and the materials have been previously described and defined by Amaral et al. elsewhere [9]. However, due to the PVC specimens' small dimensions (100x100 mm) it was necessary to place an XPS (extruded polystyrene) panel with 20 mm of thickness in the mounting ring to support the frame the openings to position the PVC specimens. Four holes were opened in the XPS panel to position the PVC specimens according to Figure 2.

Figure 2 presents the thermocouples and heat flux meter position on the specimen (in the cold and warm chambers sides). Four type-T thermocouples and four heat flux meters were mounted on PVC specimen surface faced to warm chamber side, one thermocouple type-T was embedded into the XPS panel (in the middle of the panel) and on the opposite surface faced to the cold chamber side, five thermocouple type-T in the same position were positioned.

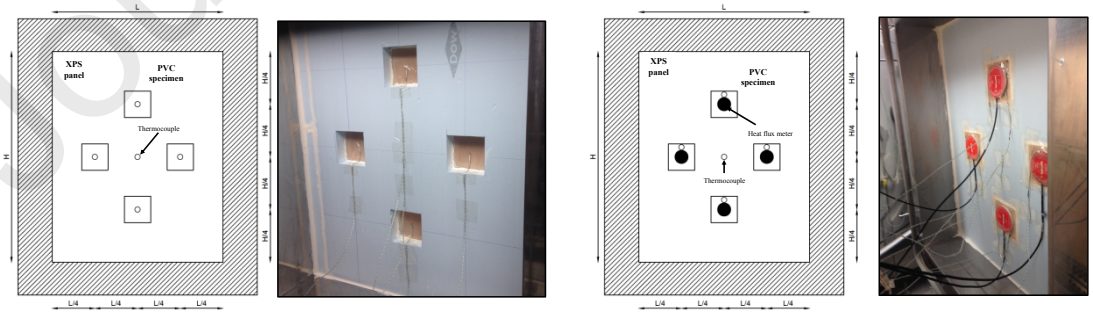

(a) Cold chamber (b) Warm chamber

Figure 2: Specimen ring mounting and sensor positioning on the surfaces of the PVC specimens

Inside both chambers (warm and cold) where positioned five PT100 probes at a distance of 150 mm from the specimen and one PT100 probe was placed in the middle of each chamber, following the instrumentation layout used in previous testing of other materials Amaral et al. [9].

The thermal conductivity (λ) is calculated according the Fourier´s Law, using Equation (2):

$$\lambda = \frac{q \times s}{\Delta T} \quad (2)$$

Where, q is the measured heat flux (W/m²) on the face of the wall specimen, s is the thickness of the wall specimen (meters) and ΔT is the temperature difference between the two wall specimens faces (°C). The sensors were calibrated and the uncertainty of each of them is ± 0.01 °C (temperature sensor), ±0.1 W/m² (heat flux sensor) and ±0.01 mm (digital calliper for specimen thickness). The uncertainty of the final thermal conductivity was associated with the propagation of uncertainty of indirect experimental measurements. The calculation of the uncertainty propagation for the thermal conductivity is ±0.017 W/m.K, according to Ricklefs et al. [48].

The thermal conductivity was calculated for different setup temperatures on the cold and warm chambers, using the same thermal amplitude value of 10 ºC and 50% of RH. The thermal conductivity was calculated for the following setup temperatures: {2;12}, {4;14}, {6;16}, {…}, {26;36}, {28;38} and {30;40} (which means: {temperature of the cold chamber in ºC; temperature of the warm chamber in ºC}). The total number of temperature steps carried out in these experimental setups was 15, and the measurement time for each temperature step was 6 hours. Although this is a method with a large experimental apparatus, the most important advantage of the use of hot box method for thermal conductivity measurements is the possibility to measure thin specimens (the case of the specimens in this study).

The thermal conductivity of the PVC layer without PCM was measured using the Hot Disk Transient Plane Source (TPS) technique [49]. The method is based on a planar sensor made of a patterned nickel element, between two composite thin layers of PVC material, like Kapton or mica. By passing current through the nickel element, and simultaneously measuring its resistivity, the sensor acts both as heater and as thermometer. By fitting the transient heating curve, estimates of thermal conductivity and diffusivity are obtained, and the specific heat calculated from the

former two. The method is standardised in ISO 22007-2 [50]. The type of sensor used in this measurement method consists of a nickel/Kapton sensor, which was placed between two similar composite thin layers. Each composite thin layer consists of 4 layers with dimensions of 40 × 40 mm (width x length) and thickness of the real specimens, this technique was only used to validate the thermal conductivity *vs* specimen temperature behaviour of the PVC without PCM using the hot box method. Therefore, hot disk measurements of the PVC layers with PCM were not performed, because the hot disk method presents some constrains for the thermal conductivity measurements with specimens incorporating PCM and for the thin specimens. The accuracy of the equipment is better than 5.0% (for thermal conductivity) according to the technical data sheet of the equipment [51].

3 Results and Discussion

3.1 Phase change materials (PCM)

3.1.1 GO functionalization with OCA

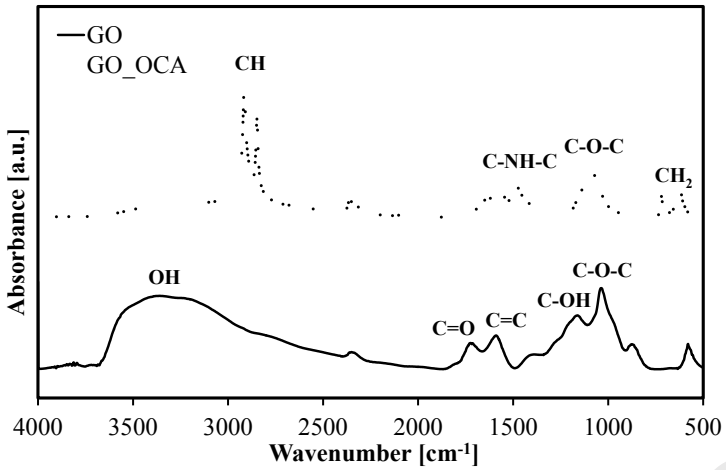

(a)

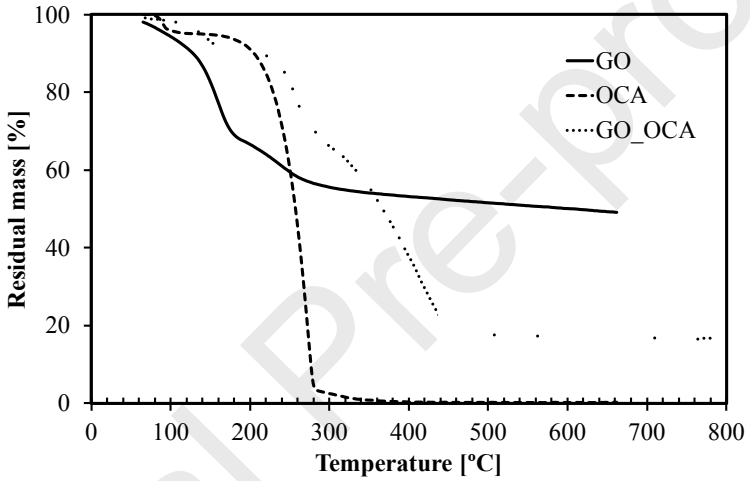

(b)

Figure 3: FTIR of GO and GO_OCA (a) and TGA thermograms (b) of OCA, GO and GO_OCA.

Figure 3 (a) shows the FTIR spectra of functionalized GO with OCA, as well as the characteristic bands of unmodified GO. The disappearance of the hydroxyl (OH) bands characteristic of GO between 3600 and 3000 cm^{-1}, together with the appearance of well-defined peaks at 2956 and 2849 cm^{-1}, associated with C–H stretching vibration indicates the presence of aliphatic chains in the GO_OCA. Also, the appearance of C-NH-C groups at 1500 cm^{-1} suggest the successfully functionalization of GO with OCA.

Figure 3 (b) shows the TGA curves of GO, functionalized GO and the aliphatic amine (OCA). The weight loss at about 100 ºC is associated with the loss of the adsorbed water, while the mass loss at 200 ºC is due to the decomposition of oxygen-containing groups from GO. At higher temperatures, 250-450 ºC, it can be observed an abrupt mass loss attributed to the decomposition of the aliphatic chains previously attached to GO.

Based on the FTIR and TGA analyses, the GO functionalization with OCA seems to have been successfully achieved. Interestingly, the thermal stability of GO_OCA was improved, and the degradation pattern significantly changed when compared to that of GO and OCA. This may be due to a synergist effect.

3.1.2 Chemical composition, morphology and microstructure of PCM

The chemical structure of the commercial PCM@BASF, the synthesized PCM@$CaCO_3$ and PCM@SiGO were assessed by FTIR, as shown in Figure 4.

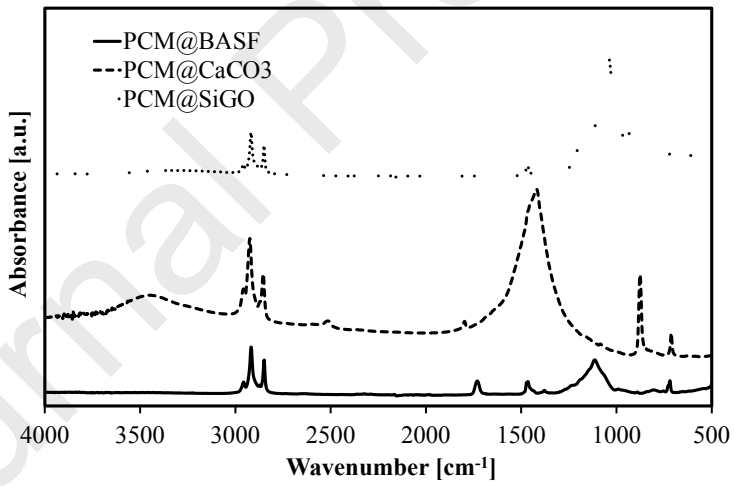

Figure 4: FTIR of PCM@BASF, PCM@$CaCO_3$ and PCM@SiGO (adapted with permission from [41]).

The commercial PCM@BASF and the synthesized PCM@$CaCO_3$ FTIR spectra's were presented and discussed previously by our group [41] and are in full agreement with what was expected. As regards the FTIR spectrum of PCM@SiGO, it presents peaks between 2956 and 2849 cm^{-1}, corresponding to the aliphatic C–H stretching vibration of paraffin and the peak at 1460 cm^{-1}, corresponding to bending vibration of CH_2. The peaks at 1044 cm^{-1} are attributed to the

asymmetrical stretching vibration of Si-O, while the peaks at 795 cm^{-1} and 424 cm^{-1} are due to the symmetrical stretching vibration of Si-O. Finally, the band at 1044 cm^{-1}, which is associated to the asymmetric stretching of the Si−O−Si bonding, confirms the presence of silica in the specimen.

The PCM morphology was analysed by SEM. Figure 5 (a) and (b) shows the morphology and the size of the PCM@BASF and PCM@$CaCO_3$ particles which have been reported elsewhere [41], while the morphology and detailed microstructure of the PCM@SiGO is shown in Figure 5 (c). From these images, it is evident the presence of the silica microspheres (20-2 μm) with some free nanoparticles (200-20 nm) deposited on their surface forming a rough and porous silica microsphere.

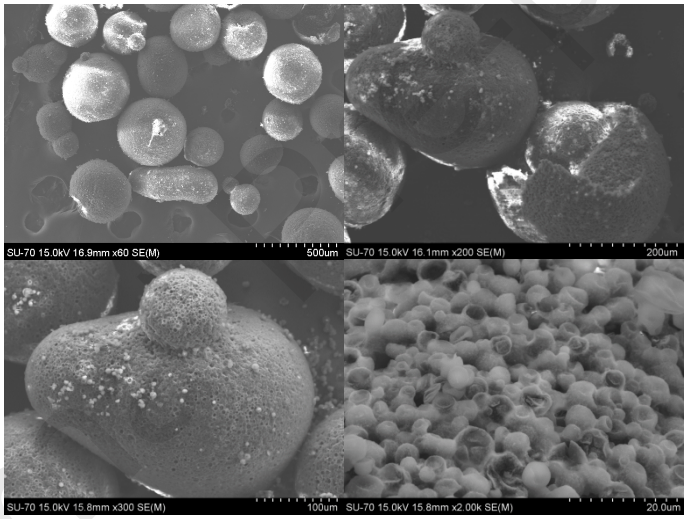

(a)

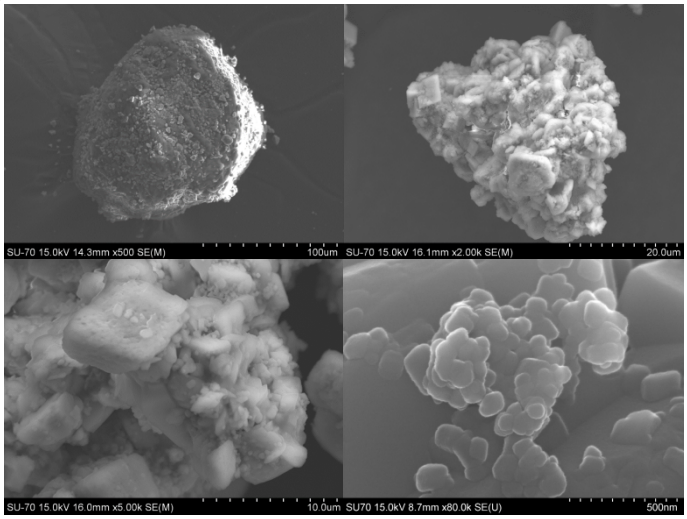

(b)

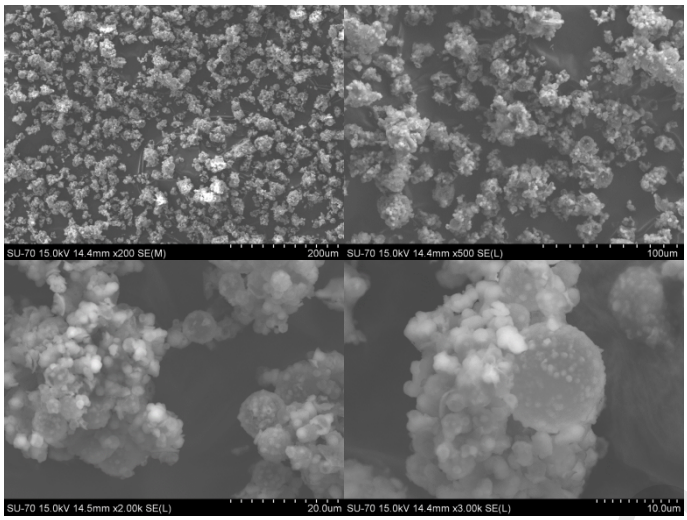

(c)

Figure 5: SEM images with different magnifications of PCM@BASF (a), PCM@$CaCO_3$ (b) and PCM@SiGO (c) (adapted with permission from [41]).

The information collected by SEM, EDX spectra and element mapping can be found in supporting information). The commercial PCM@BASF revealed that the major components are carbon (C) and oxygen (O) associated with the paraffin and the PMMA shell. The presence of silicon (Si) and sodium (Na) may be included in the polymer (PMMA) formulation as silica (SiO_2) according to Giro-Paloma et al. [52]. The synthetized PCM@$CaCO_3$ exhibited the presence of carbon (C), oxygen (O) and calcium (Ca) due to the presence of paraffin and calcium carbonate ($CaCO_3$). The small amount of sodium (Na) results from the fact that sodium carbonate was used during the synthesis,. As expect, the synthetized PCM@SiGO showed the presence of carbon (C), oxygen (O) and silicon (Si) due to the presence of paraffin and silica. The presence of GO is only inferred due to the nature of its chemical composition.

In view of the relevance that density has on the physical properties of materials, the density of the PCM was determined and the results are presented in Table 2. The PCM@SiGO has a very low density compared to the other two types of PCM. The results of the commercial PCM@BASF are in agreement with the technical data sheet of the supplier (density between 250 kg/m^3 and 350 kg/m^3) [53]. Interestingly, even though the same type of paraffin (RT18HC) and the same

paraffin/$CaCO_3$ ratio (50/50) as well as paraffin/TEOS ratio, were used, the presence of silica and GO in the synthetized PCM@SiGO lead to a considerable reduction of the density when compared to the presence of the $CaCO_3$ in the synthetized PCM@$CaCO_3$ counterpart. This may be due to various factors: on the one hand, the molar mass of $CaCO_3$ (100.087 g/mol) is higher than that of SiO_2 (60.08 g/mol); on the other hand, the presence of GO in the PCM@SiGO seems to have the effect of "expansion", forming more porous structures (consequently lighter) despite of the low GO concentration. In fact, this result is in agreement with the more porous morphology of this specimen shown in Figure 5 (c).

Table 2: Properties of the PCM

Specimens	Density (kg/m^3)	Melting		
		Transition temperature $T_{t,m}$ (°C)	Melting temperature T_m (°C)	Melting latent heat ΔH_m (J/g)
PCM@BASF	345.59±3.65	25.36±0.04	27.55±0.10	97.85±14.64
PCM@$CaCO_3$	503.36±4.39	23.37±0.65	25.84±0.44	59.56±11.78
PCM@SiGO	119.93±3.51	23.35±0.64	25.79±0.39	56.41±9.69

3.1.3 Thermal properties

Table 2 summarizes the results of the transition temperature ($T_{t,m}$), melting temperature (T_m) and latent heat (ΔH_m) values of the specimens obtained from the melting curve. As expected, the commercial PCM@BASF has considerably higher phase change enthalpy in comparison with the synthesized PCM@$CaCO_3$ and PCM@SiGO, since the synthesized PCM have less amount of paraffin. This indicates that the commercial PCM@BASF can store more latent heat when the phase change occurs. In turn, the results of both synthesized PCM are very similar, because in their formulation the same type of paraffin (RT18HC) and the same ratio (50/50) of paraffin/$CaCO_3$ and paraffin/TEOS were used. As regards the effect of the shape stabilization on

$T_{t,m}$ and T_m both lead to a reduction of about 2 ºC (8%) but the chemical characteristics of the materials used did not cause any significant impact.

Figure 6 shows the thermal stability of the commercial PCM@BASF, and of the synthesized PCM@$CaCO_3$ and PCM@SiGO.

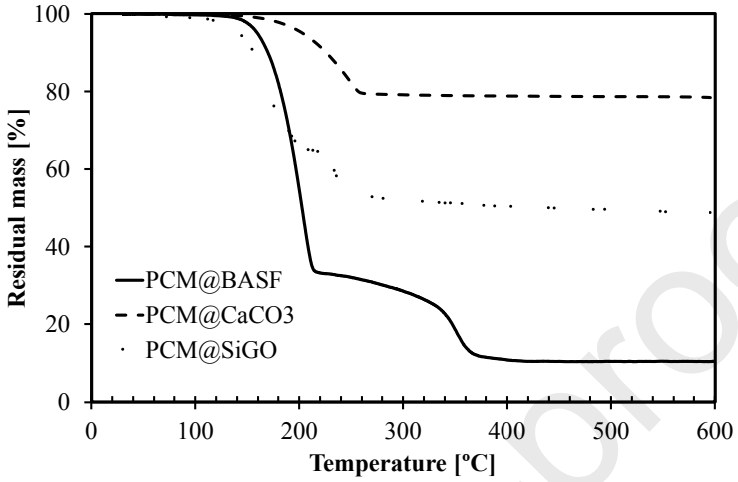

Figure 6: TGA of PCM@BASF, PCM@$CaCO_3$ and PCM@SiGO (adapted with permission from [41]).

According to Amaral et al. [41], the thermal degradation of PCM@BASF occurs in two stages, which are ascribed to the decomposition of PCM paraffin and to the decomposition of the shell material (PMMA). In turn, the thermal degradation of the synthesized PCM@$CaCO_3$, occurs in only one step, which is ascribed to the decomposition of PCM paraffin and the degradation of $CaCO_3$.

As regards the PCM@SiGO, the thermal degradation occurs in two steps. The mass loss, starting at around 100 ºC until 220 ºC, is attributed to the loss of paraffin and silica. This result is in agreement with the results presented by Zhang et al. [54]. However, in their study the mass loss of the shape-stabilized PCM with paraffin and silica occurred in a single step.

In summary, all PCM (the commercial and the synthesized) thermally stable up to 100 °C, which is above the utilization envisaged for these materials. It can also be seen that the synthesized PCM@$CaCO_3$ and PCM@SiGO decompose more slowly than the commercial PCM@BASF.

3.2 Structural layer (PVC) incorporating phase change material

Having prepared and characterized the PCM, these materials were blended with PVC and the ensuing layers characterized.

3.2.1 Morphology and mechanical properties

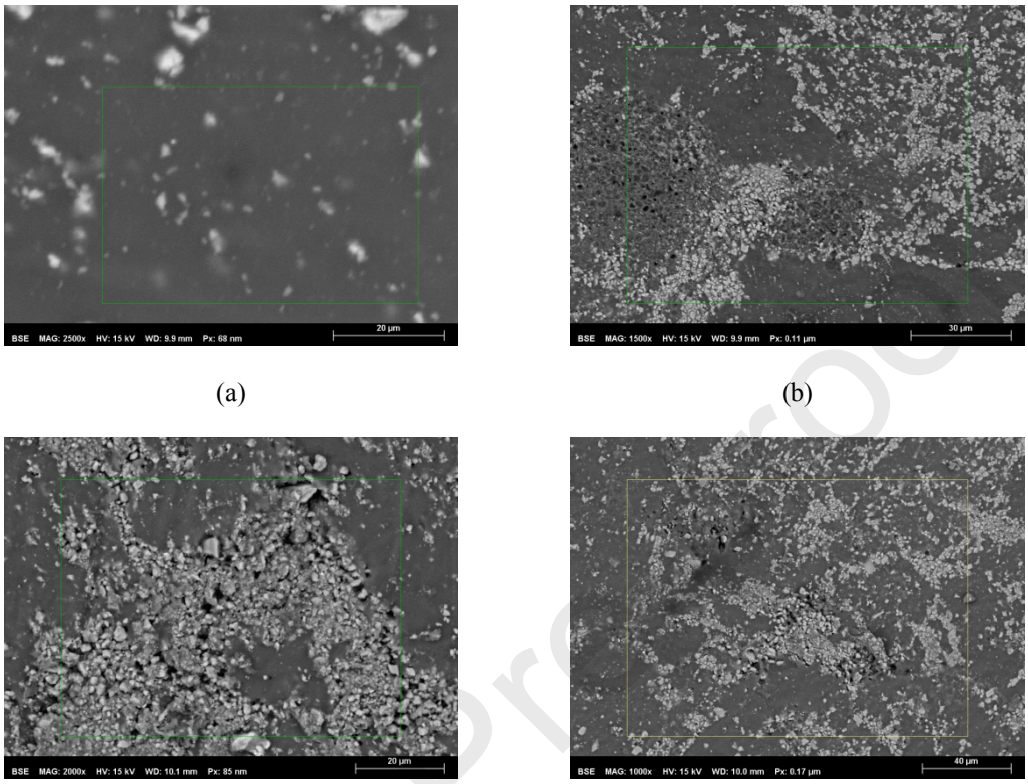

(a) (b)

(c) (d)

Figure 7: SEM images of PVC without PCM (a), PVC_5PCM@BASF (b), PVC_5PCM@$CaCO_3$ (c) and PVC_5PCM@SiGO (d)

From the SEM images presented in Figure 7, the presence of the PCM is clear. Moreover, the EDX results presented in supporting information (Figure S6) revealed that both the PVC and the composites have the same components. The major component is carbon (C) and a smaller amount of chlorine (Cl), due to the presence of PVC resin. The presence of calcium (Ca) and oxygen (O) are derived from the thermal stabilizers Ca/Zn and $CaCO_3$. However, the PVC_5PCM@BASF and PVC_5PCM@SiGO layers showed the presence of silicon (Si) due to the presence of silica (SiO_2) in the PCM formulation. In turn, the PVC_5PCM@$CaCO_3$ layer revealed the expected calcium (Ca) presence. These results are in accordance with components of the PVC and PCM formulations (see section 3.1.2).

Prior to measuring the mechanical properties of the PVC based layers, the density and the thickness were measured. The results are summarized in Table 3.

The PVC density measured for the PVC layer is in agreement with those reported in the literature for this PVC formulation (density between 1.15 g/cm^3 and 1.23 g/cm^3) [45,46]. From Table 3, it can also be observed that the density of the PVC layers increased with the incorporation of the PCMs, since the PCMs are denser materials. A similar tendency was reported by Michel et al. [55]. Moreover, the fact that the density of PVC_5PCM@SiGO layer is lower than that of the others PCM used is also reflected in the density of the ensuing PVC layers.

Table 3: Thickness, density and mechanical properties of the PVC layers with and without PCM

Specimen	Thickness (kg/m^3)	Density (kg/m^3)	Elongation at break (%)	Maximum tension (Pa)	Young´s Modulus (MPa)
PVC	1.042 ± 0.008	1256.02 ± 15.47	69.7 ± 18.2	2410.8 ± 262.7	7890.8 ± 249.8
PVC_5PCM@BASF	1.124 ± 0.044	1296.67 ± 10.79	54.2 ± 14.6	1769.8± 361.4	7251.5 ± 586.3
PVC_5PCM@$CaCO_3$	1.137 ± 0.044	1325.38 ± 15.88	34.0 ± 1.0	1403.0 ± 130.7	6892.0 ± 186.6
PVC_5PCM@SiGO	1.147 ± 0.028	1275.71 ± 18.26	38.0 ± 7.2	1337.3 ± 215.8	5866.8 ± 259.3

Next, the mechanical properties of the different PVC layers were assessed. Table 3 and Figure 8 show the tensile behaviour of the PVC layer with and without PCM, where it can be seen that the incorporation of PCM has led to the reduction of the elongation at break, maximum tension and the Young´s modulus (tensile modulus). The reduction of the mechanical performance of materials as a result of the addition of PCM was already reported in literature by Eddhahak-Ouni et al. [56]. This effect is more pronounced when the synthetized PCM, were used. However, the PVC_5PCM@SiGO layer shows slightly higher elongation at break value than the PVC_5PCM@$CaCO_3$ layer. This may be due the lower density or better dispersion of this additive in the PVC matrix.

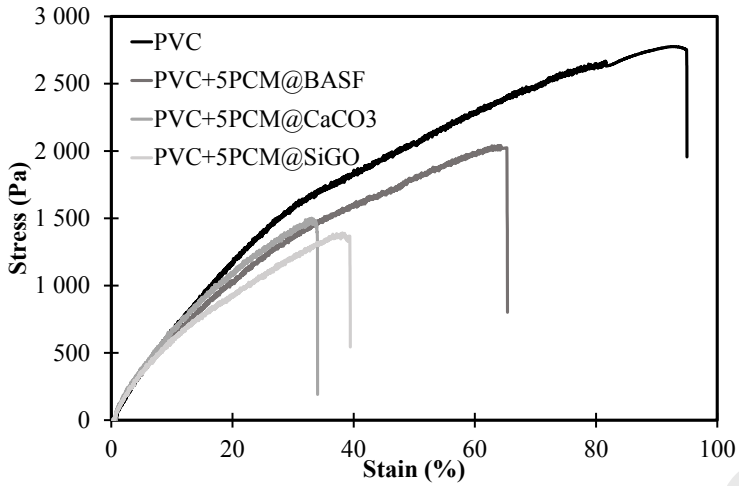

Figure 8: Stress – Strain curves the PVC layers without and with PCM

3.2.2 Thermal properties

The thermal performance of the PVC layers was assessed by DSC. Table 4 summarizes the results of the transition temperature ($T_{t,m}$), melting temperature (T_m) and latent heat (ΔH_m) values of the specimens measured on the melting curve.

Table 4: DSC results of the PVC layers with PCM

Specimens	Melting			$\%_{PCM}$
	Transition temperature $T_{t,m}$ (°C)	Melting temperature T_m (°C)	Melting latent heat ΔH_m (J/g)	
PVC_5PCM@BASF	23.39±0.16	24.93±0.16	4.25±0.82	4.3
PVC_5PCM@$CaCO_3$	23.98±0.43	24.96±1.13	3.16±0.90	5.3
PVC_5PCM@SiGO	23.35±0.64	25.07±0.29	2.66±0.29	4.7

According to the Table 4 it can be seen that the PVC layers with PCM (PVC_5PCM@BASF, PVC_5PCM@$CaCO_3$ and PVC_5PCM@SiGO) reveal an endothermic peak during heating with a small decrease in the range of values. The PVC_5PCM@BASF layer range was reduced in 2 ºC compared to the commercial PCM@BASF. The range of PVC_5PCM@$CaCO_3$ and

PVC_5PCM@SiGO layers was reduced in only 0.5 ºC compared to the synthesized PCM@$CaCO_3$ and PCM@SiGO, due to the effect of the PVC formulation and PVC layer production.

The PCM content ($\%_{PCM}$) incorporated in the PVC layer calculated according the Equation (1) was within the expected value (5.0 wt.% for the all layers). This indicates that there was no significant loss of PCM during the PVC layer production. The PVC_5PCM@BASF layer shows the highest latent heat storage capacity (4.25 J/g corresponding to 4.3 wt.%) compared to the PVC_5PCM@$CaCO_3$ layer (3.16 J/g corresponding to 5.3 wt.%) and PVC_5PCM@SiGO layer (2.66 J/g corresponding to 4.7 wt.%). Considering that the paraffin content is the same in all PCM, the lower latent heat storage capacity of the synthesized materials PCM is attributed to the inorganic stabilization materials which are responsible for the higher thermal conductivity.

Next, the thermal conductivity of the PVC layer without PCM was measured. Figure 9 illustrates the thermal conductivity *versus* temperature results using the hot disk method.

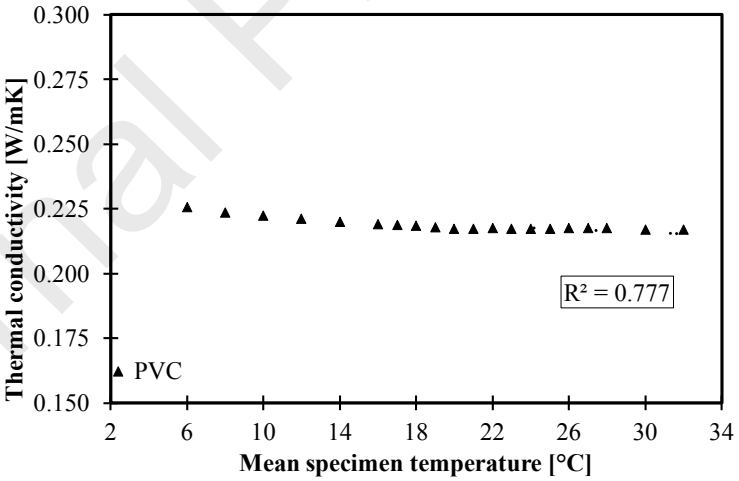

Figure 9: Thermal conductivity *versus* mean temperature of PVC layer without PCM using the hot disk method

As it can be observed, the PVC specimen without PCM presents a linear and steady decrease of thermal conductivity as the surface temperature increases. Moreover, a correlation (R^2) of 0.777, was observed. The values of the thermal conductivity were between 0.226 W/m.K (at 6 ºC) and 0.217 W/m.K (at 32 ºC). These results are consistent with the results obtained for the hot box

method. However, hot disk measurements of the PVC layers with PCM were not performed because this technique is not adequate for thin specimen especially those containing PCM as the measurement involves a combination of energy being transferred through the material and the energy stored or released during the phase change affects the thermal conductivity. Figure 10 shows the experimental data of thermal conductivity versus mean surface temperature for the PVC specimens (with and without PCM) using the hot box method.

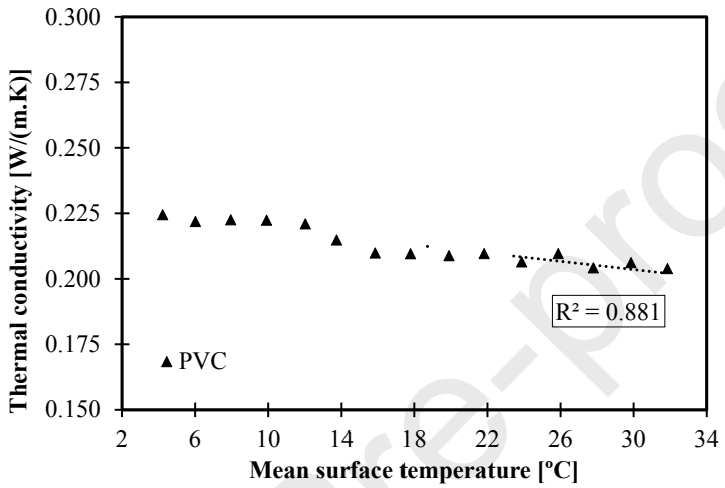

(a)

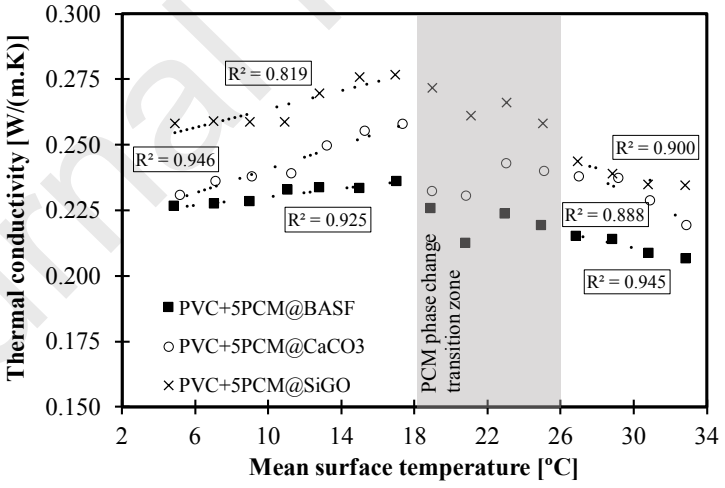

(b)

Figure 10: Thermal conductivity of the mean PVC without PCM (a) and with PCM (b) as a function surface temperature using the hot box method

According to Figure 10 (a), for the PVC layer without PCM, it can be observed that the value of the thermal conductivity decreases linearly (with a square correlation (R^2) of 0.881) as the surface temperature increases, as expected based on the results shown in Figure 9 obtained using the hot disk method. The values of the thermal conductivity were between 0.224 W/m.K (at 4.22 ºC) and 0.204 W/m.K (at 31.85 ºC).

Comparing the PVC layers with and without PCM, it can be observed that the thermal conductivity profiles are different when the mean specimen surface temperature is below and above the phase change transition range which occurs between 18 °C and 26 °C. When the mean specimen surface temperature is below the phase change transition range, the thermal conductivity increases as the surface temperature increases. Moreover, the R^2 was between 0.819 and 0.946, which demonstrates that the regression line fits reasonably well with the experimental data. In turn, when the mean specimen surface temperature is above the phase change transition range, the thermal conductivity profile shows a similar behaviour to that of the PVC layer without PCM. In this case, the thermal conductivity decreases as the surface temperature increases. Likewise, R^2 is between 0.888 and 0.945, which demonstrates that the regression line fits reasonably the experimental data. Yet, the PVC_5PCM@SiGO presents higher values compared to the PVC_5PCM@$CaCO_3$ and PVC_5PCM@BASF, which presented the expected behaviour. This enhancement of PVC_5PCM@SiGO is attributed to the high thermal conductivity of synthetized component the PCM@SiGO (the presence of GO) which allows the rapid heat transfer throughout the PVC layer.

During the PCM phase change transition (temperature range between 18 °C and 26 °C) the thermal conductivity profile of the PVC layers with PCM follows two different tendencies. A reduction followed by an increase (with the increase of mean temperature of the specimen) was observed. According to Amaral et al. [9] and Wang et al. [57] (although those experimental studies involved polyurethane foams), this behaviour is due to the coexistence of the PCM in two physical states (solid and liquid) in the phase change temperature range. Moreover, it was influenced by the temperature rise, as well as by the phase change fraction of the PCM. Furthermore, it was influenced by the fact that during PCM phase change transition, the

PVC_5PCM@SiGO layer presents higher thermal conductivity compared to the PVC_5PCM@$CaCO_3$ and PVC_5PCM@BASF layers due to the higher thermal conductivity of GO.

4 Conclusions

In this study a method to prepare PCM based on paraffin, silica and GO has been developed as well as a methodology to prepare composites based on PVC, a commercial PCM and two types of synthetized PCM. The ensuing materials have been fully characterized and noteworthy of notice is the fact that the PCM melts in a PVC network, keeping its shape.

The following main achievements can be stated:

- To improve the compatibility between paraffin and GO, GO was first functionalized with OCA. FTIR and TGA analysis confirmed the successful functionalization.
- The presence of the silica and GO in the synthetized PCM@SiGO considerably reduced the density of this material when compared to the presence of the $CaCO_3$ in the synthetized PCM@$CaCO_3$.
- SEM and the DSC results reveal that most PCM particles in the PVC layers with PCM are undamaged. Thus, both the shell (in the case of commercial PCM@BASF) and the shape stabilization materials (in the case of synthesized PCM@$CaCO_3$ and PCM@SiGO) prevent molten paraffin from leakage during the PVC layer production.
- Comparing the experimental results obtained for PVC layers with and without PCM, it was observed that the presence of PCM led to an increase in density (by the incorporation of denser fillers) and a decrease of the mechanical properties (the PCM particles create break points in PVC matrix).
- The experimental results show that the thermal conductivity decreases linearly as the surface temperature increases for the PVC layer without PCM using the hot box and hot disk methods.

- For PVC layers with PCM, the thermal conductivity profile shows a different behaviour to that of the PVC layer without PCM when the mean specimen surface temperature is below and above the phase change transition range. When the mean specimen surface temperature is below he phase change transition range, the thermal conductivity increases as the surface temperature increases. In turn, when the mean specimen surface temperature is above the phase change transition range, the thermal conductivity profile shows a similar behaviour to that of the PVC layer without PCM. However, during PCM phase change transition, the thermal conductivity profile of the PVC layers with PCM follows two tendencies. First, it was observed a reduction and then an increase with the increasing mean temperature of the specimen. Secondly, when the mean surface temperature is above the phase change transition temperature range, the thermal conductivity profile shows a decreasing tendency.

This experimental study presents promising results for the synthesized PCM@$CaCO_3$ and PCM@SiGO compared to the commercial PCM@BASF and their incorporation into the PVC layers shows potential as enhanced LHTES applications. Despite the promising results achieved, there is still a long path to fully understand the improvement of the energy storage properties and thermal conductivity of the composites as a result of adding GO to PCM. Therefore, more systematic studies are still required to select and/or develop tailor made solutions for thermal energy storage.

Acknowledgements

This work was developed under the scope of the project: MF-Retrofit – Multifunctional facades of reduced thickness for fast and cost-effective retrofitting [EeB.NMP.2013-1 Grant Agreement to: 609345] and within the scope of the project CICECO-Aveiro Institute of Materials, UIDB/50011/2020 & UIDP/50011/2020, financed by national funds through the Portuguese Foundation for Science and Technology/MCTES This work was developed within the scope of the project CICECO-Aveiro Institute of Materials, UIDB/50011/2020 & UIDP/50011/2020, financed by national funds through the Portuguese Foundation for Science

and Technology/MCTES and TEMA – Centre for Mechanical Technology and Automation, was supported by the projects UIDB/00481/2020 and UIDP/00481/2020 - FCT - Fundação para a Ciencia e a Tecnologia; and CENTRO-01-0145-FEDER-022083 - Centro Portugal Regional Operational Programme (Centro2020), under the PORTUGAL 2020 Partnership Agreement, through the European Regional Development Fund. Thanks are due to University of Aveiro, FCT/MEC for the financial support to the research Unit RISCO – Aveiro Research Centre of Risks and Sustainability in Construction (FCT/UID/ECI/04450/2013). JSA acknowledges FCT IF/01089/2015 grant.

References

[1] N. Soares, J.J. Costa, a. R. Gaspar, P. Santos, Review of passive PCM latent heat thermal energy storage systems towards buildings' energy efficiency, Energy Build. 59 (2013) 82–103. doi:10.1016/j.enbuild.2012.12.042.

[2] L. Pérez-Lombard, J. Ortiz, C. Pout, A review on buildings energy consumption information, Energy Build. 40 (2008) 394–398. doi:https://doi.org/10.1016/j.enbuild.2007.03.007.

[3] K. Pielichowska, K. Pielichowski, Phase change materials for thermal energy storage, Prog. Mater. Sci. 65 (2014) 67–123. doi:10.1016/j.pmatsci.2014.03.005.

[4] S.A. Memon, Phase change materials integrated in building walls: A state of the art review, Renew. Sustain. Energy Rev. 31 (2014) 870–906. doi:10.1016/j.rser.2013.12.042.

[5] C. Amaral, R. Vicente, P.A.A.P. Marques, A. Barros-Timmons, Phase change materials and carbon nanostructures for thermal energy storage: A literature review, Renew. Sustain. Energy Rev. 79 (2017). doi:10.1016/j.rser.2017.05.093.

[6] E. Asadi, M.G. da Silva, C.H. Antunes, L. Dias, Multi-objective optimization for building retrofit strategies: A model and an application, Energy Build. 44 (2012) 81–87. doi:https://doi.org/10.1016/j.enbuild.2011.10.016.

[7] E. Rodriguez-Ubinas, B.A. Arranz, S.V. Sánchez, F.J.N. González, Influence of the use of PCM drywall and the fenestration in building retrofitting, Energy Build. 65 (2013) 464–

476. doi:https://doi.org/10.1016/j.enbuild.2013.06.023.

[8] L.F. Cabeza, A. Castell, C. Barreneche, A. de Gracia, A.I. Fernández, Materials used as PCM in thermal energy storage in buildings: A review, Renew. Sustain. Energy Rev. 15 (2011) 1675–1695. doi:10.1016/j.rser.2010.11.018.

[9] C. Amaral, R. Vicente, V.M. Ferreira, T. Silva, Polyurethane foams with microencapsulated phase change material: Comparative analysis of thermal conductivity characterization approaches, Energy Build. 153 (2017). doi:10.1016/j.enbuild.2017.08.019.

[10] K. Biswas, Y. Shukla, A. Desjarlais, R. Rawal, Thermal characterization of full-scale PCM products and numerical simulations, including hysteresis, to evaluate energy impacts in an envelope application, Appl. Therm. Eng. 138 (2018) 501–512. doi:https://doi.org/10.1016/j.applthermaleng.2018.04.090.

[11] A. Sharma, V. V Tyagi, C.R. Chen, D. Buddhi, Review on thermal energy storage with phase change materials and applications, Renew. Sustain. Energy Rev. 13 (2009) 318–345. doi:http://dx.doi.org/10.1016/j.rser.2007.10.005.

[12] T. Silva, R. Vicente, F. Rodrigues, Literature review on the use of phase change materials in glazing and shading solutions, Renew. Sustain. Energy Rev. 53 (2016) 515–535. doi:https://doi.org/10.1016/j.rser.2015.07.201.

[13] R. Baetens, B.P. Jelle, A. Gustavsen, Phase change materials for building applications: A state-of-the-art review, Energy Build. 42 (2010) 1361–1368. doi:http://dx.doi.org/10.1016/j.enbuild.2010.03.026.

[14] B. Li, T. Liu, L. Hu, Y. Wang, L. Gao, Fabrication and Properties of Microencapsulated Paraffin@SiO2 Phase Change Composite for Thermal Energy Storage, ACS Sustain. Chem. Eng. 1 (2013) 374–380. doi:10.1021/sc300082m.

[15] M. Arıcı, F. Bilgin, S. Nižetić, H. Karabay, PCM integrated to external building walls: An optimization study on maximum activation of latent heat, Appl. Therm. Eng. 165 (2020) 114560. doi:https://doi.org/10.1016/j.applthermaleng.2019.114560.

[16] V.V. Tyagi, D. Buddhi, {PCM} thermal storage in buildings: A state of art, Renew.

Sustain. Energy Rev. 11 (2007) 1146–1166. doi:http://dx.doi.org/10.1016/j.rser.2005.10.002.

[17] G. Raam Dheep, a. Sreekumar, Influence of nanomaterials on properties of latent heat solar thermal energy storage materials – A review, Energy Convers. Manag. 83 (2014) 133–148. doi:10.1016/j.enconman.2014.03.058.

[18] L.-W. Fan, X. Fang, X. Wang, Y. Zeng, Y.-Q. Xiao, Z.-T. Yu, X. Xu, Y.-C. Hu, K.-F. Cen, Effects of various carbon nanofillers on the thermal conductivity and energy storage properties of paraffin-based nanocomposite phase change materials, Appl. Energy. 110 (2013) 163–172. doi:10.1016/j.apenergy.2013.04.043.

[19] P. Mantilla Gilart, Á. Yedra Martínez, M. González Barriuso, C. Manteca Martínez, Development of PCM/carbon-based composite materials, Sol. Energy Mater. Sol. Cells. 107 (2012) 205–211. doi:10.1016/j.solmat.2012.06.014.

[20] S. Ramakrishnan, X. Wang, J. Sanjayan, Effects of various carbon additives on the thermal storage performance of form-stable PCM integrated cementitious composites, Appl. Therm. Eng. 148 (2019) 491–501. doi:https://doi.org/10.1016/j.applthermaleng.2018.11.025.

[21] F. Kuznik, D. David, K. Johannes, J.-J. Roux, A review on phase change materials integrated in building walls, Renew. Sustain. Energy Rev. 15 (2011) 379–391. doi:http://dx.doi.org/10.1016/j.rser.2010.08.019.

[22] Y. Konuklu, M. Unal, H.O. Paksoy, Microencapsulation of caprylic acid with different wall materials as phase change material for thermal energy storage, Sol. Energy Mater. Sol. Cells. 120 (2014) 536–542. doi:10.1016/j.solmat.2013.09.035.

[23] a. Jamekhorshid, S.M. Sadrameli, M. Farid, A review of microencapsulation methods of phase change materials (PCMs) as a thermal energy storage (TES) medium, Renew. Sustain. Energy Rev. 31 (2014) 531–542. doi:10.1016/j.rser.2013.12.033.

[24] C.Y. Zhao, G.H. Zhang, Review on microencapsulated phase change materials (MEPCMs): Fabrication, characterization and applications, Renew. Sustain. Energy Rev. 15 (2011) 3813–3832. doi:10.1016/j.rser.2011.07.019.

[25] Y.P. Zhang, K.P. Lin, R. Yang, H.F. Di, Y. Jiang, Preparation, thermal performance and application of shape-stabilized PCM in energy efficient buildings, Energy Build. 38 (2006) 1262–1269. doi:10.1016/j.enbuild.2006.02.009.

[26] G.-Q. Qi, C.-L. Liang, R.-Y. Bao, Z.-Y. Liu, W. Yang, B.-H. Xie, M.-B. Yang, Polyethylene glycol based shape-stabilized phase change material for thermal energy storage with ultra-low content of graphene oxide, Sol. Energy Mater. Sol. Cells. 123 (2014) 171–177. doi:10.1016/j.solmat.2014.01.024.

[27] M. Mehrali, S.T. Latibari, M. Mehrali, H.S.C. Metselaar, M. Silakhori, Shape-stabilized phase change materials with high thermal conductivity based on paraffin/graphene oxide composite, Energy Convers. Manag. 67 (2013) 275–282. doi:10.1016/j.enconman.2012.11.023.

[28] M. Vivekananthan, V.A. Amirtham, Characterisation and thermophysical properties of graphene nanoparticles dispersed erythritol PCM for medium temperature thermal energy storage applications, Thermochim. Acta. 676 (2019) 94–103. doi:https://doi.org/10.1016/j.tca.2019.03.037.

[29] Z. Jiang, W. Yang, F. He, C. Xie, J. Fan, J. Wu, K. Zhang, Modified Phase Change Microcapsules with Calcium Carbonate and Graphene Oxide Shells for Enhanced Energy Storage and Leakage Prevention, ACS Sustain. Chem. Eng. 6 (2018) 5182–5191. doi:10.1021/acssuschemeng.7b04834.

[30] Y. Qu, S. Wang, Y. Tian, D. Zhou, Comprehensive evaluation of Paraffin-HDPE shape stabilized PCM with hybrid carbon nano-additives, Appl. Therm. Eng. 163 (2019) 114404. doi:https://doi.org/10.1016/j.applthermaleng.2019.114404.

[31] M.M. Umair, Y. Zhang, K. Iqbal, S. Zhang, B. Tang, Novel strategies and supporting materials applied to shape-stabilize organic phase change materials for thermal energy storage–A review, Appl. Energy. 235 (2019) 846–873. doi:https://doi.org/10.1016/j.apenergy.2018.11.017.

[32] C. Wang, L. Feng, W. Li, J. Zheng, W. Tian, X. Li, Shape-stabilized phase change materials based on polyethylene glycol/porous carbon composite: The influence of the

pore structure of the carbon materials, Sol. Energy Mater. Sol. Cells. 105 (2012) 21–26. doi:https://doi.org/10.1016/j.solmat.2012.05.031.

[33] N. Zhu, S. Li, P. Hu, S. Wei, R. Deng, F. Lei, A review on applications of shape-stabilized phase change materials embedded in building enclosure in recent ten years, Sustain. Cities Soc. 43 (2018) 251–264. doi:https://doi.org/10.1016/j.scs.2018.08.028.

[34] J. Hu, W. Chen, Y. Qu, D. Yang, Safety and serviceability of membrane buildings: A critical review on architectural, material and structural performance, Eng. Struct. 210 (2020) 110292. doi:https://doi.org/10.1016/j.engstruct.2020.110292.

[35] P.K.S. Rathore, S.K. Shukla, Potential of macroencapsulated PCM for thermal energy storage in buildings: A comprehensive review, Constr. Build. Mater. 225 (2019) 723–744. doi:https://doi.org/10.1016/j.conbuildmat.2019.07.221.

[36] V.V. Tyagi, S.C. Kaushik, S.K. Tyagi, T. Akiyama, Development of phase change materials based microencapsulated technology for buildings: A review, Renew. Sustain. Energy Rev. 15 (2011) 1373–1391. doi:10.1016/j.rser.2010.10.006.

[37] D. Feldman, M.M. Shapiro, P. Fazio, A heat storage module with a polymer structural matrix, Polym. Eng. Sci. 25 (1985) 406–411. doi:10.1002/pen.760250705.

[38] X. Jin, J. Li, P. Xue, M. Jia, Preparation and characterization of PVC-based form-stable phase change materials, Sol. Energy Mater. Sol. Cells. 130 (2014) 435–441. doi:https://doi.org/10.1016/j.solmat.2014.07.013.

[39] Y. Chen, L. Zhao, Y. Shi, Preparation of polyvinyl chloride capsules for encapsulation of paraffin by coating multiple organic/inorganic layers, J. Taiwan Inst. Chem. Eng. 77 (2017) 177–186. doi:https://doi.org/10.1016/j.jtice.2017.04.046.

[40] Y. Wang, S. Ge, B. Huang, Z. Zheng, A simple route to PVC encapsulated Na2SO4·10H2O nano/micro-composite with excellent energy storage performance, Mater. Chem. Phys. 223 (2019) 723–726. doi:https://doi.org/10.1016/j.matchemphys.2018.11.075.

[41] C. Amaral, S.C. Pinto, T. Silva, F. Mohseni, J.S. Amaral, V.S. Amaral, P.A.A.P. Marques, A. Barros-Timmons, R. Vicente, Development of polyurethane foam incorporating phase

change material for thermal energy storage, J. Energy Storage. 28 (2020) 101177. doi:https://doi.org/10.1016/j.est.2019.101177.

[42] O.D. Neikov, N.A. Yefimov, Chapter 1 - Powder Characterization and Testing, in: O. Neikov, S. Naboychenko, N.V.B.T.-H. of N.-F.M.P. (Second E. Yefimov (Eds.), Elsevier, Oxford, 2019: pp. 3–62. doi:https://doi.org/10.1016/B978-0-08-100543-9.00001-4.

[43] PerkinElmer, Diamond Differencial Scanning Calorimeter (DSC), (2003). https://web.itu.edu.tr/~yusuf/labs/DSC.pdf.

[44] NETZSCH, STA 449 F3 Jupiter, (n.d.). https://www.netzsch-thermal-analysis.com/en/products-solutions/simultaneous-thermogravimetry-differential-scanning-calorimetry/sta-449-f3-jupiter/.

[45] N. Gama, R. Santos, B. Godinho, R. Silva, A. Ferreira, Triacetin as a Secondary PVC Plasticizer, J. Polym. Environ. 27 (2019) 1294–1301. doi:10.1007/s10924-019-01432-z.

[46] N. V Gama, R. Santos, B. Godinho, R. Silva, A. Ferreira, Methyl Acetyl Ricinoleate as Polyvinyl Chloride Plasticizer, J. Polym. Environ. 27 (2019) 703–709. doi:10.1007/s10924-019-01383-5.

[47] SHIMADZU, AGS-X Series (Specifications table-top), (n.d.). https://www.shimadzu.com/an/test/universal/ags-x/specifications.html.

[48] A. Ricklefs, A.M. Thiele, G. Falzone, G. Sant, L. Pilon, Thermal conductivity of cementitious composites containing microencapsulated phase change materials, Int. J. Heat Mass Transf. 104 (2017) 71–82. doi:https://doi.org/10.1016/j.ijheatmasstransfer.2016.08.013.

[49] S.E. Gustafsson, Transient plane source techniques for thermal conductivity and thermal diffusivity measurements of solid materials, Rev. Sci. Instrum. 62 (1991) 797–804. doi:10.1063/1.1142087.

[50] ISO 22007-2: Plastics - Determination of thermal conductivity and thermal diffusivity - Part 2: Transient plane heat source (hot disc) method, (2015). https://www.iso.org/standard/61190.html.

[51] HOTDISK, TPS 2500 S: Hot Disk Thermal Constants Analyser, (n.d.).

https://thermtest.com/wp-content/uploads/2500S.pdf.

[52] J. Giro-Paloma, G. Oncins, C. Barreneche, M. Martínez, A.I. Fernández, L.F. Cabeza, Physico-chemical and mechanical properties of microencapsulated phase change material, Appl. Energy. 109 (2013) 441–448. doi:https://doi.org/10.1016/j.apenergy.2012.11.007.

[53] BASF, Micronal® PCM: Intelligent Temperatura Management for Buildings, (2008). www.micronal.de.

[54] Y. Zhang, S. Zheng, S. Zhu, J. Ma, Z. Sun, M. Farid, Evaluation of paraffin infiltrated in various porous silica matrices as shape-stabilized phase change materials for thermal energy storage, Energy Convers. Manag. 171 (2018) 361–370. doi:https://doi.org/10.1016/j.enconman.2018.06.002.

[55] B. Michel, P. Glouannec, A. Fuentes, P. Chauvelon, Experimental and numerical study of insulation walls containing a composite layer of PU-PCM and dedicated to refrigerated vehicle, Appl. Therm. Eng. 116 (2017) 382–391. doi:https://doi.org/10.1016/j.applthermaleng.2016.12.117.

[56] A. Eddhahak-Ouni, S. Drissi, J. Colin, J. Neji, S. Care, Experimental and multi-scale analysis of the thermal properties of Portland cement concretes embedded with microencapsulated Phase Change Materials (PCMs), Appl. Therm. Eng. 64 (2014) 32–39. doi:https://doi.org/10.1016/j.applthermaleng.2013.11.050.

[57] X. Wang, H. Yu, L. Li, M. Zhao, Research on temperature dependent effective thermal conductivity of composite-phase change materials (PCMs) wall based on steady-state method in a thermal chamber, Energy Build. 126 (2016) 408–414. doi:https://doi.org/10.1016/j.enbuild.2016.05.058.

Highlights

- Poly(vinyl chloride) (PVC) structural layer incorporating phase change materials (PCM);
- Shape stable PCM based on paraffin, silica and graphene oxide has been developed;
- Improving the thermal characteristics of PVC layers with different types of PCM;